

Experimental investigation into unstable two phase flow phenomena during flow boiling in multi-microchannels

LY, Yuanzheng, XIA, Guodong, CHENG, Lixin and MA, Dandan

Available from Sheffield Hallam University Research Archive (SHURA) at:

<https://shura.shu.ac.uk/28450/>

This document is the Accepted Version [AM]

Citation:

LY, Yuanzheng, XIA, Guodong, CHENG, Lixin and MA, Dandan (2021). Experimental investigation into unstable two phase flow phenomena during flow boiling in multi-microchannels. *International Journal of Thermal Sciences*, 166. [Article]

Copyright and re-use policy

See <http://shura.shu.ac.uk/information.html>

Experimental investigation into unstable two phase flow phenomena during flow boiling in multi-microchannels

Yuanzheng Lv^a, Guodong Xia^{a*}, Lixin Cheng^{a,b} and Dandan Ma^a

^a *Key Laboratory of Enhanced Heat Transfer and Energy Conservation, Ministry of Education, Beijing University of Technology, Beijing 100124, China*

^b *Department of Engineering and Mathematics, Sheffield Hallam University, Howard Street, Sheffield S1 1WB, UK*

Abstract

Experiments of unstable vapor liquid two phase flow phenomena during flow boiling with HFE-7100 in two parallel rectangular multi-microchannels with aspect ratios of 0.2364 and 0.3182 were conducted under a wide range of test conditions: the mass flux from 380 to 3500 kg/m²s, the heat flux from 0 to 1080 kW/m² and the compressive volumes of 0, 5, 10 and 20 ml, respectively. First, characteristics of flow boiling heat transfer and two-phase pressure drop in the two parallel multi-microchannels are compared with each other. It shows that the maximum dissipated heat flux in the microchannels with the aspect ratio of 0.3182 is 34.4% larger than that in the microchannels with the aspect ratio of 0.2364 while the pressure drop in the microchannels with higher aspect ratio is up to 80% less than that in the microchannels with lower aspect ratio under the test conditions.

1

*Corresponding author: Tel.: +86 10 67391985-8301;

fax: +86 10 67391983.

Email address: xgd@bjut.edu.cn

Then, experimental results of unstable vapor liquid two phase processes in the two parallel multi-microchannels are compared with each other. It shows that the minimum heat flux decreases with decreasing the aspect ratio at the same compressive volumes. Finally, the physical mechanisms of unstable vapor liquid two phase phenomena in the parallel multi-microchannels have been analyzed according to a simplified mathematical model based on the mass and momentum conservation. It is concluded that a wide flat regime in the hydrodynamic curves may decrease the unstable vapor liquid two phase flow phenomena.

Keywords: Microchannels; unstable vapor liquid two phase flow; flow boiling; flow patterns; pressure drop oscillation.

1. Introduction

Microchannel cooling technology plays an important role in removing high heat flux in aerospace, automotive, micro-electronics, energy, fuel cells and so on [1]. For one example, with the rapid development of high performance chips in micro-electronics industry, improving integration level and packaging density is important to high performance of chips but also generates extremely high heat flux density [2]. For another example, fuel cells which are an attractive efficient technology for clean energy utilization generate high heat fluxes as well. The effective cooling methods are important for increasing service life of the relevant critical device in fuel cells as pointed out by Wang [3]. Due to the confined spaces, parallel multi-microchannels are generally used in fuel cells and are becoming a cutting-edge technology for heat transfer and fluid flow in many engineering

applications but there are also big challenges associated with their use [4-7]. Understanding the fluid flow and thermal management in the parallel multi-microchannels is critical in the fuel cell scale-up [3, 5]. Furthermore, microchannel cooling technology becomes a cutting-edge technology for heat transfer and fluid flow in many engineering applications but there are also big challenges due to the complex phenomena and underlying physical mechanisms [4-7]. Besides the channel size, shape, surface condition, fluid physical properties and operation parameters, understanding the flow boiling and two phase instability is a very important part in understanding the complex phenomena, physical mechanisms and technology development but is not yet well understood. Therefore, it is essential to conduct experimental research on this important topic and to further explore the physical mechanisms governing the very complex unstable flow boiling heat transfer and two phase phenomena.

Flow boiling heat transfer of HFE-7100 (the saturation temperature is 61°C at 1 atm) in microchannels is a promising approach to cooling electronic chips and fuel cells and has been widely investigated [2, 8]. The generation, growth and combination of bubbles can disturb the thermal layers drastically, and together with the latent heat of vaporization, the heat transfer coefficient in flow boiling process can be very high, and the wall temperature distributes uniformly [9-11]. Moreover, for flow boiling in microchannels, the liquid flow rate is smaller than that for single phase flow for the same thermal load in general [12]. However, the disadvantages of flow boiling in microchannels are prominent as well. The flow boiling and two phase instability can cause severe pressure drop oscillation between the inlet and the outlet of microchannels [13-16], and the intermittent hotspots on the channel wall, which possibly lead to control issues or safety issues [17]. Thus, it is essential to experimentally investigate the unstable flow boiling of HFE-7100 in different structural

microchannels under a wide range of test conditions in order to advance knowledge and theory in the relevant topics.

Quite different characteristics and mechanisms of unstable vapor liquid two phase flow phenomena during flow boiling exist in both macrochannels and microchannels [18]. The upstream compressive volume could be caused by the elastic pipeline, residual gas and so on. The fluid in microchannels can exchange momentum with the fluid in the upstream compressive volume, leading to two phase pressure drop oscillation. Furthermore, the density wave oscillation is caused by the periodic changing of the density of fluid in the microchannels. The complex phenomena of changes of bubbles and flow patterns in the confined channels may also cause flow boiling instabilities [19]. The parallel interaction oscillation between the parallel multi-microchannels is caused by the nonuniform flow distribution. The pressure drop oscillation has much longer cycles and larger amplitudes in comparison to the density wave oscillation and the parallel interaction oscillation [4, 20, 21]. As for microchannels, their hydraulic diameters are less than 200 μm , so the strong restriction due to the microchannel confinement on flow boiling and two phase flow has a notable effect on unstable vapor liquid two phase flow phenomena during flow boiling in microchannels [22]. The backflow, high superheated degree and thermal conduction along the microchannel wall make the flow boiling and two phase flow phenomena and physical mechanisms in the microchannels much more complex than that in the macrochannels [16, 18, 23 - 25]. Once the unstable flow boiling is triggered by some disturbances such as the sudden expansion of bubbles, the self-sustaining oscillation in pressure drop, wall temperature and mass flow rate will begin.

Both experimental and theoretical studies have been conducted over the past years. In the experimental aspect, Liu et. al [26] experimentally studied the effect of the inlet compressibility on

flow boiling heat transfer coefficient using water and n-hexane as the working fluid. Their results show that flow boiling heat transfer coefficient depends on the mass flux but does not depend on the wall heat flux for a lower upstream compressive volume while flow boiling heat transfer coefficient depends on the heat flux but does not depend on the mass flux for a larger upstream compressive volume. Decreasing the compressive volume in the upstream may improve the flow boiling stability and heat transfer rates. Qu and Mudawar [20] experimentally investigated the effect of flow restriction using an inlet valve at the upstream side of the test section on flow boiling instability. Their experimental results show that pressure drop oscillation with long cycle and large amplitude can be reduced significantly when the flow was highly restricted using the inlet valve. That is to say, if the upstream compressive volume cannot be changed, increasing the upstream flow resistance is helpful to improve the flow boiling stability. In the theoretical aspect, Zhang et. al [27] developed a dynamic model for simulating the pressure drop oscillation using water as the working fluid. The dynamic model considers both the compressive volume and the hydrodynamic characteristic curve (a pressure drop versus flow-rate curve at constant thermal loads) of the working fluid. When the working fluid is boiling in the microchannels under a constant thermal load, the pressure drop of microchannels has a complex relation with flow rates. The pressure drop increases with increasing the flow rate at first, then drops, and then increases again. Such a hydrodynamic characteristic can be simplified as a cubic curve. The simulation results have good agreement with the experimental results, and it has been found that the negative slope zone leads to the momentum exchange of the working fluid between the microchannel and the compressive volume and the experimental results have shown that the variation of frictional pressure drop makes the hydrodynamic characteristic curve become a cubic curve [26, 27]. According to the research of Chiapero et. al [28], the negative

slope zone can be affected by the way of heating and the inlet subcooling degree. In particular, the negative differential zone could be eliminated by significantly increasing the operating pressure and the pumping power, thus, microchannels with an inlet restriction have been proposed to eliminate instable flow boiling and two phase flow [9, 29-31]. In practical application, a long pipeline ($L/d > 150$) or liquid tank in the upstream of boiling microchannels could provide some compressive volume [32], which means that the eliminating the compressive volume may not be practical [33]. As such, new types of microchannels with diverging structures, reentrant cavities, fins and segmented structures have been proposed and the flow boiling processes are quite stable in such microchannels [9, 34-39]. Obviously, such complex structures can only affect the upstream compressibility to some extent, especially the general trend that the pressure drop declines with increasing the mass flux at constant heating power condition is not affected. The compressive volume in the upstream pipeline, however, seems not to work in such cases.

According to the afore-going literature review, some available methods to reducing unstable vapor liquid two phase flow phenomena during flow boiling in microchannels have been proposed, but quantitative research on the relation between the upstream compressive volume and the hydrodynamic characteristic of the working fluid is still needed. Therefore, the present study focuses on experiments, mathematical model and mechanistic analysis of the unstable vapor liquid two phase flow phenomena and the physical mechanisms during flow boiling in the two parallel multi-microchannels having different aspect ratios with the same width of $220\ \mu\text{m}$ and two different depths of $52\ \mu\text{m}$ and $70\ \mu\text{m}$. The compressive volume in the upstream of the pipeline was adjusted by a nitrogen vessel (0, 5, 10, 20 ml). The flow boiling, flow resistance and hydrodynamic characteristic curves in the two parallel multi-microchannels have been analyzed according to the

measured results and observed phenomena. The oscillations of pressure drop, wall temperature, mass flux and two-phase distribution in unstable boiling at different compressive volumes have been observed. The flow boiling instability maps in the multi-microchannels with the two different aspect ratios are presented. The physical mechanisms have been proposed by analyzing the simplified mathematical model for the unstable vapor liquid two phase flow during flow boiling in the multi-microchannels. Furthermore, the relations between the unstable flow boiling and vapor liquid two phase processes and the average slope of the negative slope zone in the hydrodynamic characteristic curves are discussed and explained according to the underlying physical mechanisms.

2. Experimental setup and test section

2.1. Experimental setup

The schematic diagram of the flow boiling experimental system is shown in Fig. 1. The working fluid is HFE-7100 and the purity of which can be greater than 99.6% after degassing and distillation. HFE-7100 was stored in the liquid tank first, and then driven into the pipeline by a high-precision plunger pump. Once the liquid tank was filled with HFE-7100, the entire liquid loop should be isolated from atmosphere to prevent air from dissolving into it. The working fluid flowed through a nitrogen vessel, a preheater, a mass flow rate transmitter and a test section. The test section was heated using cartridge heaters inserted in an aluminium block. The heating power of the test section was controlled by a digital DC (direct current) power supply. The two-phase mixture flowing out of the test section was cooled by a condenser. Then, the subcooled working fluid flowed back into the liquid tank. The inlet temperature of the working fluid was set at 25°C and 37.5°C respectively, so

the subcooled degree of the inlet was -36°C and -23.5°C . There was a monophasic length in the microchannels, which depended on the test mass flow rate and heating power set up in the experiments and can be determined according to the energy balance of the specific test conditions. The nitrogen vessel with a scale was used to simulate the upstream compressibility. Before the experiments were started, the target volume (0, 5, 10 or 20 mL) of nitrogen was injected into the nitrogen vessel at 1 atm. A pressure drop transmitter (Rosemount 3051, USA) was used to measure the pressure drop between the inlet and the outlet of the microchannels. A mass flow rate transmitter (Alicat LC, USA) was used to measure the mass flow rate in the system. A high-speed microscope (Keyence VW-9000, Japan) was used to record the two-phase distribution in the microchannels. The inlet and outlet fluid temperatures T_{in} and T_{out} were measured by a pair of high-precision K type thermocouples, which were calibrated by a standard mercury thermometer with an accuracy of 0.05 K. As shown in Fig. 2, two holes for installing the thermocouples are in the right and left heat isolation shells, respectively. The two holes are deep enough and towards to the microchannels' inlet and outlet precisely and thermocouples installed in the two holes were used to measure the inlet and outlet fluid temperatures. Thermocouples were installed in the test section to measure the wall temperatures and their variations. All the signals were collected by a data acquisition system (Agilent 34970A, USA) and stored digitally for future analysis.

2.2. Test section

Two parallel rectangular multi-microchannels with aspect ratios of 0.3182 and 0.2364 were used as the test section in the experiments. The substrates of both microchannels are made of 6063 aluminium alloy, which were machined by the laser engraving method and with a high-accuracy

CNC (Computer Numerical Control) work table. As shown in Fig. 2 (a), the chamber for the cartridge heater was machined at the lower end of the heater block. All of the thermocouples were inserted in the heater block up to the center line of the heat block. Thermocouples T11, T12, T13, and T14 were 0.5 mm distance from the bottom of the microchannels, which were used to measure the wall temperatures in the flow direction. The wall temperature measured with thermocouples T22, T23, T32, and T33 was used to calculate the total heating power based on the Fourier's law of heat conduction.

Table 1 shows the structural parameters of the two multi-microchannels. Both multi-microchannels have the same width of 220 μm but have different depths. The depth of first microchannels (MC 1) is 70 μm , and the depth of the second microchannels (MC 2) is 34.2% shallower than the first microchannels at 52 μm . The two microchannels are referred to as MC 1 and MC 2, respectively. The dimension inspection has shown that the biggest section area difference is only 6.7% in MC 1 and MC 2. The four tapped holes on the bottom surface of the substrate are designed for fixing the quartz glass as shown in Fig. 2 (b). The polyethylene terephthalate (PET) film between the upper surface of ribs and the glass has a thickness of 10 μm , which can protect the quartz glass by weakening the concentration of stresses and prevent the single/two-phase flow between fins and glass. As such, the fluid flow may be considered as uniform distribution in the present experimental work. Two Teflon shells with O-rings and screw bolts ensure good sealing of the test section. Each shell has holes for installing the pipeline and sensors as shown in Fig. 2 (b).

3. Data reduction and measurement uncertainties

The thermophysical and transport properties of HFE-7100 were obtained from REFPROP Version 8.0 [40]. For example, the thermophysical and transport properties of HFE-7100 at 101.3 kPa are shown in Table 2. The test mass flux is from 200 to 2000 kg/m²s. The mass flux (G) is determined as follows:

$$G = \frac{m}{NA_{mc}} \quad (1)$$

where m is the measured mass flow rate, and A_{mc} is the area of one single microchannel.

The main structure of the aluminium alloy substrate and the heating module installed in the test section are similar to those in our previous research [33]. According to the experiment results and discussion in the our previous work [33], this design of substrate can ensure that the heat flow differences are less than $\pm 5\%$ even for the long flow channels. Therefore, the heat flow can be considered as uniform distribution in the experiments.

Maranzana et al. [41] have proposed a non-dimensional parameter M . According to the algorithms of M , if the value of M is less than 0.01, the effect of the axial heat conduction in the heat sink is insignificant. The M values for MC 1 and MC 2 are 0.0025 and 0.0027, respectively. The effect of external factors on the axial heat conduction in the heat sink has decreased to the minimum. Therefore, the axial heat conduction in the microchannels can be ignored in the present study. The total heating power (P_{total}) can be calculated based on the Fourier's law of heat conduction as follows:

$$P_{total} = \frac{\lambda_a A_{cs}}{\Delta H_{2,3}} \Delta T_{2,3} \quad (2a)$$

$$\Delta T_{2,3} = \frac{T_{32} + T_{33}}{2} - \frac{T_{23} + T_{22}}{2} \quad (2b)$$

where λ_a is the thermal conductivity of 6063 aluminum alloy, A_{cs} is the base area of the substrate ($W \times L$), and $\Delta H_{2,3}$ is the height difference between T_{22} , T_{23} and T_{32} , T_{33} . The effective power (P_{eff}) and the heat loss power (P_{loss}) can be calculated when the microchannels are occupied by single phase heat transfer as follows:

$$P_{eff} = N c_p G A_{mc} (T_{out} - T_{in}) \quad (3a)$$

$$P_{loss} = P_{total} - P_{eff} \quad (3b)$$

where T_{out} and T_{in} are the fluid temperatures at inlet and outlet of microchannels, and c_p is the specific heat of the working fluid at the average temperature of the inlet and outlet temperatures. The heat loss power decreases with the increase of the heat transfer coefficient, the heat loss power under the conditions of the three different mass fluxes were measured and fitted into equations 4(a) - (c) as follows:

$$P_{loss} = 0.0701 P_{total} - 0.00189 \quad \text{for } G = 507.4 \text{ kg/m}^2\text{s} \quad (4a)$$

$$P_{loss} = 0.0592 P_{total} + 0.0039 \quad \text{for } G = 1501.5 \text{ kg/m}^2\text{s} \quad (4b)$$

$$P_{loss} = 0.0554P_{total} - 0.00811 \text{ for } G = 3100.4 \text{ kg/m}^2\text{s} \quad (4c)$$

The heat transfer coefficient of single phase forced convection generally has a positive relation with the mass flux. According to the Eq. 4(a)-(c), it can be found that the heat loss power decreases with increasing the mass flux, or the heat transfer coefficient, but the decreasing rate of the heat loss is declining. For all mass fluxes in the experiments, the average heat loss is about 5.85% of the total heating power. The effective base heat flux in the substrate (q_{base}) and the wall temperature near the outlet can be written as one-dimensional form:

$$q_{base} = \frac{P_{eff}}{A_{cs}} \quad (5a)$$

$$T_{w,4} = T_{14} - \frac{\Delta H}{\lambda_a} q_{base} \quad (5b)$$

where the ΔH is the height between the bottom surface of the microchannels and T14 which is 0.5 mm.

The effective wall heat flux and the local heat transfer coefficient can be calculated based on the fin efficiency with adiabatic tips (η) as described in our previous works [9, 42]. The calculation methods are shown as follows:

$$q_{eff} = \frac{P_{eff}}{A_r} \quad (6a)$$

$$A_r = NL_{mc}(W_{mc} + 2\eta D_{mc}) \quad (6b)$$

$$h = \frac{q_{eff}}{T_w - T_f} \quad (6c)$$

The vapour quality at the outlet of the microchannels can be determined according to the energy balance as follows [20]:

$$x_{out} = \frac{mh_{in} + P_{eff}}{mh_{lg}} \quad (7)$$

where h_{in} is the enthalpy of the working fluid at the inlet of the microchannels. The void fraction [16] at the outlet can be written as:

$$\alpha = \frac{1}{1 + \left(\frac{1 - x_{out}}{x_{out}} \right) \left(\frac{\rho_g}{\rho_l} \right)^{2/3}} \quad (8)$$

Eq. (8) was derived from the principle of minimum entropy production proposed by Zivi [43]. According to the research, the idealized slip-ratio in Eq. (8) is $(\rho_l/\rho_g)^{1/3}$. Qu and Mudawar [20] proposed a pressure drop prediction method for microchannels and used Eq. (8) in their method for microchannel flow boiling and have proved that Eq. (8) is reliable in their study. Therefore, Eq. (8) is used to calculate the void fraction in the present study.

The pressure drop between the inlet and outlet of the microchannels is determined as follows:

$$\Delta p_{mc} = (p_{IN} - p_{OUT}) - (\Delta p_{sc} + \Delta p_{se}) \quad (9)$$

where p_{IN} and p_{OUT} are the measured inlet and outlet pressures respectively. Δp_{sc} and Δp_{se} are the pressure losses caused by the sudden contraction at the inlet and the sudden expansion of the outlet respectively. According to the study by Xia et al. [22], the calculation methods for local pressure losses recommended by Qu and Mudawar [20] are adopted in the present study. The microchannels are horizontal, thus the gravitational pressure drop is zero. The acceleration pressure drop can be calculated as follows:

$$\Delta p_a = \frac{G^2}{\rho_l} \left[\frac{x_{out}^2}{\alpha_{out}} \left(\frac{\rho_l}{\rho_g} \right) + \frac{(1-x_{out})^2}{1-\alpha_{out}} - 1 \right] \quad (10)$$

Consequently, the frictional pressure drop can be written as follows:

$$\Delta p_f = \Delta p_{mc} - \Delta p_a \quad (11)$$

The relative uncertainties of parameters above were calculated based on the Holman methods of uncertainty analysis [17, 44]. Table 3 shows the summary of the uncertainties of the measured parameters and derived parameters in the present study.

4. Experimental procedure and results

4.1. Experimental procedure

In the upstream before the test section, small air bubbles in the liquid and the compressibility of the nitrogen vessel might generate some compressive volume into the upstream of the test section. The diameter of the upstream pipe (d_p) is 6 mm and the length (L_{mp}) of the pipe is 160 mm. The ratio of L_{mp} to d_p is less than 150, therefore, the compressibility due to this part is weak [32]. Some small air bubbles might occur in the system due to the residual air in the upstream pipeline [45]. Before the experiments, the pipeline was rinsed by running high flow rate to eliminate the air bubbles in the experimental system. When there were no visible air bubbles observed by a microscope for at least 30 min, the experimental system was used for the experiments. The compressibility of the nitrogen vessel was controlled by changing the volume of nitrogen. The nitrogen was injected into vessel after the pump was stopped and the local pressure of vessel was 1 atm. This ensured the measurement accuracy of the nitrogen volume used in the experiments. After the preparation, the experiments were conducted according to the planned test runs in the experiments.

4.2. Characteristics of flow boiling heat transfer and two-phase flow resistance of HFE-7100 in the multi-microchannels

Figure 3 shows the comparisons of flow boiling curves and flow resistance characteristics of HFE-7100 in MC 1 and MC 2. In the experiments, the inlet temperature was set at 25°C at first, so the subcooled degree of inlet was -36°C. The mass flux G ranged from 608.8 to 1561.2 kg/m²s, and the effective heating flux ranged from 0 to 1080 kW/m². In both channels MC 1 and MC 2, variations of the time-average wall temperature (T_w) had similar trends. The slopes of boiling curves are quite small when the microchannels are mainly occupied by the single phase forced convection,

and then increase when flow boiling occurs. At $G = 811.7 \text{ kg/m}^2\text{s}$ and $T_w = 80^\circ\text{C}$ in the two microchannels, the dissipated heat flux of MC 2 is 34.4% lower than that of MC 1, but the frictional pressure drop in MC 2 is 80% higher than that of MC 1. By comparison, at the working conditions of $G = 1561.2 \text{ kg/m}^2\text{s}$ and $T_w = 80^\circ\text{C}$ in the two microchannels, the dissipated heat fluxes become 31.4% and 29.1%, respectively. Moreover, MC 2 has lower heat flux and higher pressure drop than MC 1 at the same mass flow rate ($m = 7.5 \times 10^{-5} \text{ kg/s}$) and time-average wall temperature (80°C) as shown in Fig. 3 (a) and (b).

The differences of heat transfer rates and pressure drops between the two microchannels are closely related to the flow patterns in the two multi-microchannels. At $G = 608.8 \text{ kg/m}^2\text{s}$, $q_{eff} = 240.5 \text{ kW/m}^2$ and vapor quality at the outlets around 0.4, the two-phase distributions in MC 1 and MC 2 are shown in Fig. 4. As for MC 1, the upstream is mainly dominated by the bubbly flow, and these bubbles are generated from the side and bottom surfaces in rapid succession. Some of them merged together or directly expanded to larger size bubbles, and then became washed away by the liquid. Some bubble nucleation phenomena are observed at intermediate of channels as well. All bubbles were flowing and elongating at the same time, so the downstream of MC 1 was mainly dominated by annular flow. The liquid films were measured by the measurement software of VW-9000 microscope, which range from 7 to 22 μm . The two-phase distribution in MC 2, however, is much simpler in comparison with MC 1. In the upstream of the microchannels, the newly generated bubbles expanded towards both the upstream and the downstream rapidly and fiercely, and many small bubbles were wiped away before detaching from the wall surfaces. The downstream of MC 2 exhibits annular flow as well, but the liquid film ranges from 29 to 51 μm due to the small cross section area. The comparative results of heat transfer coefficients at the outlets of MC 1 and MC 2 are shown in Fig. 5.

It is noted that the average flow boiling heat transfer coefficient of HFE-7100 in MC 2 is lower than that MC 1's by 41.1% at the low mass fluxes and vapor qualities. The rapidly expanding bubbles blocked the channels and reduced the heat transfer of HFE-7100 by impeding the nucleate boiling. However, at the high vapor qualities, the flow patterns in both channels are annular flow, but dryout in MC 1 occurred more readily due to the thinner liquid film and bigger hydraulic diameter as compared to those in MC 2. Therefore, MC 2 has higher heat transfer coefficients than MC 1.

4.3. Comparison of the unstable vapor liquid two phase flow phenomena during flow boiling in the two multi-microchannels

Figure 6 (a) shows the characteristic curves of the vapor liquid two phase pressure drop of HFE-7100 in MC 1 and MC 2 respectively. The inlet temperature is 25°C, and the effective heat fluxes are 426.1 kW/m² and 672.8 kW/m². The mass flow rate ranges from 7.5×10⁻⁵ to 3.1×10⁻⁴ kg/s. The mass fluxes in the two multi-microchannels range from 710 to 3300 kg/m²s for MC 1 and 380 to 2500 kg/m²s for MC 2 respectively. At a constant effective heat flux, with increasing the mass flux, the pressure drops in both MC 2 and MC 1 increase at first, then decrease and finally increase again. The pressure drop decreases due to the decrease of the vapor quality.

As shown in Fig. 6 (a), the outlet vapor quality x_{out} in the negative slope regime basically ranges from 1 to 0. The hydrodynamic characteristic curve is supposed to be a third order function $f(G)$, so the negative slope ($df(G)/dG$) of a certain G in the declining regime can be written as follows:

$$\frac{df(G)}{dG} = -s \frac{kPa}{kg/m^2s} \quad (12)$$

where s is the numerical value of the local slope, and its unit is $\text{kPa}/(\text{kg}/\text{m}^2\text{s})$.

The average negative slopes (s_a) in the decreasing region in MC 1 and MC 2 can be fitted and calculated based on the experimental data. Figure 6 (b) demonstrates the variations of the average negative slopes (s_a) with effective heat flux in MC 1 and MC 2. The parametric trends of s_a in MC 2 and MC 1 are similar but s_a in MC 2 is 43% smaller than that in MC 1. Obviously, decrease in the aspect ratio has a significant effect on the change of flow characteristics of the microchannels, and such characteristic differences can also affect the unstable flow boiling processes. By adjusting the nitrogen volume in the vessel, unstable flow boiling phenomena have been observed. Figure 7 shows the oscillations of the mass flux, the pressure drop and the wall temperature in MC 1 and MC 2 at $V_{N_2} = 5 \text{ ml}$, $T_{in} = 25^\circ\text{C}$, $q_{eff} = 672.8 \text{ kW}/\text{m}^2$ and $G = 1564.5 \text{ kg}/\text{m}^2\text{s}$. Although the average negative slope in MC 2 at $q_{eff} = 672.8 \text{ kW}/\text{m}^2$ is about 200% higher than that in MC 1, the oscillation period in MC 2 is only 10% longer than that in MC 1, and the wave forms of various measured parameters are similar. However, the amplitudes of the mass flux and the pressure drop in MC 2 are 50% higher than those in MC 1. The inlet temperature changed little in MC 1 while the peak value of the inlet temperature in MC 2 could be as high as 37.5°C . The vapor was also observed to be reversing to the inlet chamber. In addition, the average wall temperature in MC 1 oscillated around 80°C while the average wall temperature in MC 2 was about 93°C due to the heat transfer deterioration and high saturated temperature of the working fluid caused by the pressure oscillation. By comparison, the mass flux, pressure drop and wall temperature did not oscillate at the working conditions of $V_{N_2} = 0 \text{ ml}$, $T_{in} = 25^\circ\text{C}$, $q_{eff} = 672.8 \text{ kW}/\text{m}^2$ and $G = 1564.5 \text{ kg}/\text{m}^2\text{s}$. As shown in Fig. 8, all the parameters are almost constant.

The unstable flow boiling maps have been obtained according to the experiment results at $V_{N_2} =$

5 – 20 ml, $T_{in} = 25^{\circ}\text{C}$, $q_{eff} = 0 - 1200 \text{ kW/m}^2$ and $G = 211 - 2100 \text{ kg/m}^2\text{s}$ as shown in Figs. 9 (a) and (b), respectively. The oscillations of various parameters in MC 1 and MC 2 occur at $x_{out} = 0.32 - 0.95$ and $x_{out} = 0.38 - 0.96$, respectively, which are quite similar. However, the minimum effective heat fluxes for the unstable flow boiling in MC 1 and MC 2 at the same compressive volume are quite different. At the volume of nitrogen $V_{N_2} = 5 \text{ ml}$, the minimum effective heat fluxes in MC 1 and MC 2 are 540 kW/m^2 and 520 kW/m^2 , respectively. When V_{N_2} is increased to 10 ml, the minimum effective heat flux is 475 kW/m^2 in MC 1 and is 175 kW/m^2 in MC 2. When V_{N_2} is increased to 20 ml, the minimum effective heat flux is 180 kW/m^2 in MC 1. It indicates that decrease in s_a makes the unstable flow boiling processes in the microchannels more sensitive and drastic. Therefore, optimizing the structures of the microchannels to reduce the unstable flow boiling phenomena by using the highest s_a is recommended according to the measured results and analysis.

5. Analysis and mechanisms of unstable flow boiling phenomena in the multi-microchannels

The limiting mechanism of the unstable flow boiling phenomena is the momentum exchange between the fluid in the microchannels and the fluid in nitrogen vessel. The flow boiling experimental system in the present study may be simplified to the flow boiling model with a compressive volume as shown in Fig. 10. The simplified model consists of the nitrogen vessel and the microchannels. This model may be used to analyze the relation between s_a and flow boiling stability. The inlet total mass flow rate is m_0 , the inlet mass flow rate of microchannels is m_{mc} , and the m_v is the mass flow rate flowing into the nitrogen vessel. The following equation can be written according to mass conservation for the model:

$$m_0 = m_v + m_{mc} \quad (13)$$

According to the conservation of momentum, the equation between the inlet pressure of the microchannels (p_{in}) and the pressure of N₂ (p_{N2}) can be written as follows:

$$p_{in} - p_{N2} = \frac{H_v}{A_v} \frac{dm_v}{dt} \quad (14)$$

where H_v is the height difference between the upper surface of liquid in the nitrogen vessel and the microchannels, A_v is the cross-section area of the nitrogen vessel. The relation between the inlet pressure (p_{in}) and the outlet (p_{out}) pressure of the microchannels can be written as follows:

$$p_{in} - p_{out} = \frac{L_{mc}}{NA_{mc}} \frac{dm_{mc}}{dt} + f(m_{mc}) \quad (15)$$

where $f(m_{mc})$ is the idealized hydrodynamic curve of HFE-7100 at a constant heat flux and is considered as a cubic curve.

The differential form of $f(m_{mc})$ can be written as follows:

$$\frac{df(m_{mc})}{dm_{mc}} = \alpha(m_{mc} - m_{max})(m_{mc} - m_{min}) \quad (16)$$

where m_{max} and m_{min} are the inflection mass flow rates of the hydrodynamic curve of HFE-7100,

and α is a fitting coefficient greater than 0.

Nitrogen is considered as an ideal gas, therefore, p_{N_2} can be written as follows:

$$p_{N_2} = \frac{C}{V_{N_2}} \quad (17)$$

where C is a constant value. Change of m_v will change the volume of nitrogen (V_{N_2}), the change rate of V_{N_2} can be written as follows:

$$\frac{dV_{N_2}}{dt} = -\frac{m_v}{\rho} \quad (18)$$

Therefore, the differential form to time change of Eq. (17) is as follows:

$$\frac{dp_{N_2}}{dt} = \frac{p_{N_2}}{\rho V_{N_2}} m_v = \Omega m_v \quad (19)$$

where the Ω is a parameter varying inversely with the compressive volume. Combining with the Eqs. (13) – (16), and (19), a second order balanced differential equation can be obtained as follows:

$$Z \frac{dm_{mc}^2}{dt} + \alpha(m_{mc} - m_{\min})(m_{mc} - m_{\max}) \frac{dm_{mc}}{dt} + \Omega(m_{mc} - m_0) = 0 \quad (20a)$$

$$Z = \frac{H_v}{A_v} + \frac{L_{mc}}{NA_{mc}} \quad (20b)$$

Assuming $y_1 = m_{mc} - m_0$ and $y_2 = dy_1/dt$, Eq. (20a) may be expressed as follows:

$$\frac{dy_1}{dt} = y_2 \quad (21a)$$

$$\frac{dy_2}{dt} = \frac{\alpha}{Z}(y_1 + m_0 - m_{\min})(m_{\max} - m_0 - y_1)y_2 - \frac{\Omega}{Z}y_1 \quad (21b)$$

In Eqs. (21a) and (21b), the status of $y_1 = 0$ and $y_2 = 0$ is balanced, but the stability at this status is judged by the eigenvalues. At the $(0, 0)$ status, the Jacobi matrix ($\mathbf{J}_{(0,0)}$) of Eqs. (21a) and (21b) can be written as follows:

$$\mathbf{J}_{(0,0)} = \begin{bmatrix} 0 & 1 \\ -\frac{\Omega}{Z} & \frac{\alpha}{Z}\omega \end{bmatrix} \quad (22a)$$

$$\omega = (m_0 - m_{\min})(m_{\max} - m_0) \quad (22b)$$

where ω represents the relation between m_0 and two inflection mass flow rates. If m_0 is right in the middle between m_{\min} and m_{\max} , then ω will reach the maximum. If m_0 is equal to m_{\min} or m_{\max} , then ω will be 0. In other cases, ω will be less than 0. Therefore, the eigenmatrix $|\lambda\mathbf{E} - \mathbf{J}_{(0,0)}|$ can be written as follows:

$$|\lambda\mathbf{E} - \mathbf{J}_{(0,0)}| = \begin{vmatrix} \lambda & -1 \\ \frac{\Omega}{Z} & \lambda - \frac{\alpha}{Z}\omega \end{vmatrix} = \lambda^2 - \frac{\alpha}{Z}\omega\lambda + \frac{\Omega}{Z} = 0 \quad (23)$$

The solutions to Eq. (23) can be calculated as follows:

$$\lambda_1 = \frac{\alpha\omega + \sqrt{\alpha^2\omega^2 - 4\Omega^2}}{2Z} \quad (24a)$$

$$\lambda_2 = \frac{\alpha\omega - \sqrt{\alpha^2\omega^2 - 4\Omega^2}}{2Z} \quad (24b)$$

If the outlet vapor quality x_{out} is less than 1 in the flow boiling, m_0 must be located between m_{min} and m_{max} . The difference between $\alpha\omega$ and Ω determines the solutions distribution of Eq. (23) according to Eqs. (24a) and (24b). These solutions can directly judge the stability at balanced status. As stated in Eqs. (16), (19) and (22b), the parameters α , ω , Ω and Z are greater than 0. So, the product of α and ω actually weighs the degree of negative slope at the certain balanced status when the working conditions of heat flux and inflection mass flow rates are given. In the meanwhile, the parameter Ω reflects the compressive degree in the upstream of microchannels.

The relationship between the upstream compressibility in the multi-microchannels and the negative slope of hydrodynamic curve essentially determines the stability of the balanced status. For example, in the first case, when the hydrodynamic curve of working fluid is given and the upstream of the microchannels has a lower compressibility, the product of α and ω will be less than 2Ω , and the solutions to Eq. (23) will be a pair of conjugate complex numbers with positive real parts. The balanced status $(0, 0)$ is unstable and the various parameters will oscillate around the balanced status. However, in the second case, when the upstream of the microchannels has a higher compressibility, the product of α and ω will be greater than or equal to 2Ω , the solutions are one or two positive real

numbers, so the system status will continually deviate from the balanced status but without oscillation.

According to the instability-evaluating model proposed by Lee et al. [46], the non-dimensional parameter R for judging instability can be written as follows:

$$R = \sqrt{\frac{F_{back}}{F_{forward}}} = \frac{P}{2A_{mc}h_g G} \sqrt{\frac{\rho_l}{\rho_g}} \quad (25)$$

where R is the ratio of the backward evaporation momentum force (F_{back}), and the forward liquid inertia force ($F_{forward}$). If the R value is less than unity, even though there are multiple channels, all the channels will be stable. When the instability parameter R is greater than unity, every channel could be fluctuated. The parameter R also indicates that the flow boiling stability will get worse when the width of channel is kept constant but aspect ratio decreases. That is to say, MC 1 is more stable than MC 1 when the surface tension, latent heat and so on of working fluid are the same. The differences between the experimental and simulated results have proved it. The experimental data and the calculated results are shown in Fig. 11 (a) and (b), respectively. At $V_{N2} = 5$ ml, $T_{in} = 25^\circ\text{C}$, $q_{eff} = 514.1$ kW/m² and $G = 1344.1$ kg/m²s, the mass flux in MC 1 oscillates sharply at $t = 0 - 300$ s, and then stabilizes at the set value gradually in 20 minutes. At $t = 0 - 300$ s, the computed amplitudes and periods favorably agree with the experimental results, but the computed waveform is distorted severely. Moreover, the computed mass flux doesn't stop spontaneously, that is different with the experimental observations. Although the idealized hydrodynamic curve is provided with the advantages of convenience and speed when dealing with most of the unstable flow boiling problem, its own defect should not be ignorable: at the working conditions of a low effective heat flux as

shown in Fig. 6 (a), the curve with sharply declining rate only occupies a very small part in the negative slope regime, and the remaining parts are flat. The curve with the sudden change is hard to be fitted, and there must be some distortions between the fitting curve and the actual one. Figure 12 shows the R-squared (R^2) of fitting curve and the R^2 represents the fitting accuracy. It is found that the fit quality (R^2) improves as s_a decreases in both MC 1 and MC 2. When the s_a is smaller than -0.1, the R^2 is closed to 1, which indicates that the actual curves are reasonably fitted by cubic curves. When s_a is higher than -0.1, however, the fitting accuracy is lower than 0.95, which indicating that the fitting starts to deviate from the real curve. Consequently, the unstable analysis methods described by Eqs. (21) - (24) may generate big differences. The wide flat part in the negative regime may be used to reduce the unstable flow boiling phenomena, even though the average negative slope is small.

6. Conclusions

Experimental, mathematical and mechanistic investigation of the unstable two phase flow phenomena during flow boiling of HFE-7100 in the two parallel rectangular multi-microchannels with two different aspect ratios were conducted in the present study. The pressure drops and the wall temperature oscillations were measured and the corresponding flow patterns were captured with the high-speed microscope. The unstable flow boiling phenomena in the two multi-microchannels were compared with each other. Furthermore, the mechanisms of the unstable two phase phenomena are analyzed according to the simplified mathematical model. The main conclusions from the present research are summarized as follows:

For stable flow boiling at the same working conditions, the heat transfer coefficients of HFE-7100 in MC 1 are more than 50% higher than that in MC 2, and the two phase pressure drops in MC 1 are 80% lower than that in MC 2. The effect of the aspect ratio has a significant effect on the flow boiling heat transfer and pressure drop characteristics. Furthermore, the observed flow patterns in MC 1 are small bubbly and annular flow while they are elongated bubbly and annular flow in MC 2. This is mainly due to the strong effect of the confinement on the flow regimes in MC 2. The reversing stream also blocks the microchannels and leads to high two phase pressure drop.

The average negative slope in the hydrodynamic characteristic curves decreases with decreasing the aspect ratio of the microchannels at a constant heat flux. MC 2 is 33 % shallower than MC 1, and its average negative slope is 45% higher than that of MC 1. Furthermore, the negative slope of the hydrodynamic characteristic curve is inversely proportional to the heat flux.

For unstable flow boiling at the same working conditions, the fluctuation amplitudes of the mass flux and the pressure drop in MC 2 are more than 50% higher than those in MC 1, but the periods in the two multi-microchannels are similar. Due to the reversing of stream, the inlet temperature in MC 2 oscillates with increasing the mass flux. The smaller average negative slope makes the microchannels more sensitive for the compressive volume change.

A simplified mathematical model based on the mass and momentum conservations has been proposed for the flow boiling in the multi-microchannels. According to the analysis, the variation of slope in the hydrodynamic characteristic curve has a significant effect on the flow boiling instability in the multi-microchannels. The wide flat part in the negative slope zone may enhance the flow boiling stability. The hydrodynamic characteristic curve with the small average negative slope and sudden change is hard to be fitted by the cubic curve for $s_a > 1$, which greatly affects the computed

results using the unstable flow boiling model.

The relationship between the upstream compressibility in the microchannels and the negative slope of hydrodynamic curve essentially determines the stability of the balanced status. MC 1 is more stable than MC 1 when the surface tension, latent heat and so on of working fluid are the same. The differences between the experimental and simulated results in the present study have proved this conclusion.

Acknowledgements

This work was supported by the National Natural Science Foundation of China (No. 51976002).

Nomenclatures

A	area, m^2
A_r	total heat transfer area of microchannels, m^2
A_{cs}	the cross section area of substrate, m^2
A_v	the cross section area of nitrogen vessel, m^2
c_p	specific heat at constant pressure, $J/(kg \cdot K)$
D_h	hydraulic diameter, m
D_{mc}	depth of the microchannels, m
d_p	diameter of pipeline, m
f	a third order function

G	mass flux, kg/m ² s
ΔH	height difference between T11 and microchannels, m
$\Delta H_{2,3}$	height difference between thermocouples, m
h	heat transfer coefficient, W/m ² K
h_{in}	enthalpy at the inlet, kJ/kg
h_{out}	enthalpy at the outlet, kJ/kg
h_{lg}	latent heat, kJ/kg
L	length, m
m	mass flow rate, kg/s
N	number of channels
W	width, m
P	heating power, W
P_{total}	total heating power, W
P_{eff}	effective heating power, W
P_{loss}	power of heat loss, W
P	pressure, kPa
Δp	pressure difference, kPa
q	heat flux density, W/m ² s
q_{eff}	effective heat flux density, W/m ²
q_{base}	effective heat flux density through the substrate, W/m ²
s	slope, kPa/(kg/m ² s)
s_a	average slope, kPa/(kg/m ² s)

T	temperature, °C
$\Delta T_{2,3}$	temperature difference between thermocouples, °C
t	time, s
V	volume, m ³
x_{out}	vapor quality of outlet
y	variable
Z	the ratio of length to cross section area

Greek symbols

α	the fitting coefficient
η	the ribs' efficiency
λ	thermal conductivity, W/(m·K)
μ	kinematic viscosity, Pa·s
ρ	density, kg/m ³
Σ	total value
Ω	the compressive coefficient
ω	mass flow rate coefficient

Subscripts

a	aluminum alloy
-----	----------------

cs	cross section of the substrate
in	inlet
IN	inlet of test section
loss	heat loss
mc	microchannel
mp	main pipeline
max	maximum
min	minimum
N ₂	nitrogen
out	outlet
OUT	outlet of test section
r	rib
s	substrate
sc	sudden contraction
se	sudden expansion
sp	springe pump
w	wall

References

[1] I. Mudawar, Two-Phase Microchannel Heat Sinks: Theory, Applications, and Limitations, Journal of Electronic Packaging, 133 (2011) 041002.

- [2] T.G. Karayiannis, M.M. Mahmoud, Flow boiling in microchannels: Fundamentals and applications, *Applied Thermal Engineering*, 115 (2017) 1372-1397.
- [3] J. Wang, Theory and practice of flow field designs for fuel cell scaling-up: A critical review ☆, *Applied Energy*, 157 (2015) S0306261915000380.
- [4] J. Xu, J. Zhou, Y. Gan, Static and dynamic flow instability of a parallel microchannel heat sink at high heat fluxes, *Energy Conversion and Management*, 46 (2005) 313-334.
- [5] J. Wang, H. Wang, Flow-Field Designs of Bipolar Plates in PEM Fuel Cells: Theory and Applications, *Fuel Cells*, 12 (2012) 989-1003.
- [6] J. Xu, G. Liu, W. Zhang, Q. Li, B. Wang, Seed bubbles stabilize flow and heat transfer in parallel microchannels, *International Journal of Multiphase Flow*, 35 (2009) 773-790.
- [7] F. Barreras, A. Lozano, J. Barroso, V. Roda, M. Maza, Theoretical Model for the Optimal Design of Air Cooling Systems of Polymer Electrolyte Fuel Cells. Application to a High-Temperature PEMFC, *Fuel Cells*, 13 (2013) 227-237.
- [8] E.J. Choi, J.Y. Park, M.S. Kim, Two-phase cooling using HFE-7100 for polymer electrolyte membrane fuel cell application, *Applied Thermal Engineering*, 148 (2019) 868-877.
- [9] Y. Li, G. Xia, Y. Jia, Y. Cheng, J. Wang, Experimental investigation of flow boiling performance in microchannels with and without triangular cavities – A comparative study, *International Journal of Heat and Mass Transfer*, 108 (2017) 1511-1526.
- [10] W. Li, K. Zhou, J. Li, Z. Feng, H. Zhu, Effects of heat flux, mass flux and two-phase inlet quality on flow boiling in a vertical superhydrophilic microchannel, *International Journal of Heat and Mass Transfer*, 119 (2018) 601-613.
- [11] W. Li, Z. Wu, A general criterion for evaporative heat transfer in micro/mini-channels,

International Journal of Heat and Mass Transfer, 53 (2010) 1967-1976.

[12] L. Cheng, G. Xia, Fundamental issues, mechanisms and models of flow boiling heat transfer in microscale channels, International Journal of Heat and Mass Transfer, 108 (2017) 97-127.

[13] H. Huang, L.M. Pan, R.G. Yan, Flow characteristics and instability analysis of pressure drop in parallel multiple microchannels, Applied Thermal Engineering, 142 (2018) S1359431118312249-.

[14] C.A. Chávez, N.O. Moraga, G. Ribatski, Thermal oscillations during flow boiling of hydrocarbon refrigerants in a microchannels array heat sink, Applied Thermal Engineering, 157 (2019) 113725.

[15] S. Chen, X. Chen, G. Luo, K. Zhu, L. Chen, Y. Hou, Flow boiling instability of liquid nitrogen in horizontal mini channels, Applied Thermal Engineering, 144 (2018) 812-824.

[16] L. Yin, P. Jiang, R. Xu, W. Wang, L. Jia, Visualization of flow patterns and bubble behavior during flow boiling in open microchannels, International Communications in Heat and Mass Transfer, 85 (2017) 131-138.

[17] G. Xia, Y. Lv, L. Cheng, D. Ma, Y. Jia, Experimental study and dynamic simulation of the continuous two-phase instable boiling in multiple parallel microchannels, International Journal of Heat and Mass Transfer, 138 (2019) 961-984.

[18] Y.K. Prajapati, P. Bhandari, Flow boiling instabilities in microchannels and their promising solutions – A review, Experimental Thermal and Fluid Science, 88 (2017) 576-593.

[19] A. Tamanna, P.S. Lee, Flow boiling instability characteristics in expanding silicon microgap heat sink, International Journal of Heat and Mass Transfer, 89 (2015) 390-405.

[20] W. Qu, I. Mudawar, Measurement and prediction of pressure drop in two-phase micro-channel heat sinks, International Journal of Heat and Mass Transfer, 46 (2003) 2737-2753.

- [21] R. Khodabandeh, R. Furberg, Instability, heat transfer and flow regime in a two-phase flow thermosyphon loop at different diameter evaporator channel, *Applied Thermal Engineering*, 30 (2010) 1107-1114.
- [22] G. Xia, Y. Lv, D. Ma, Y. Jia, Experimental investigation of the continuous two-phase instable boiling in microchannels with triangular corrugations and prediction for instable boundaries, *Applied Thermal Engineering*, 162 (2019) 114251.
- [23] S. Hong, Y. Tang, Y. Lai, S. Wang, An experimental investigation on effect of channel configuration in ultra-shallow micro multi-channels flow boiling: Heat transfer enhancement and visualized presentation, *Experimental Thermal and Fluid Science*, 83 (2017) 239-247.
- [24] H. Li, P.S. Hrnjak, Effect of channel geometry on flow reversal in microchannel evaporators, *International Journal of Heat and Mass Transfer*, 115 (2017) 1-10.
- [25] D. Bogojevic, K. Sefiane, G. Duursma, A.J. Walton, Bubble dynamics and flow boiling instabilities in microchannels, *International Journal of Heat and Mass Transfer*, 58 (2013) 663-675.
- [26] Y. Liu, D.F. Fletcher, B.S. Haynes, On the importance of upstream compressibility in microchannel boiling heat transfer, *International Journal of Heat and Mass Transfer*, 58 (2013) 503-512.
- [27] T. Zhang, J.T. Wen, Y. Peles, J. Catano, R. Zhou, M.K. Jensen, Two-phase refrigerant flow instability analysis and active control in transient electronics cooling systems, *International Journal of Multiphase Flow*, 37 (2011) 84-97.
- [28] E. Manavela Chiapero, D. Doder, M. Fernandino, C.A. Doraio, Experimental parametric study of the pressure drop characteristic curve in a horizontal boiling channel, *Experimental Thermal and Fluid Science*, 52 (2014) 318-327.

- [29] G. Wang, P. Cheng, A.E. Bergles, Effects of inlet/outlet configurations on flow boiling instability in parallel microchannels, *International Journal of Heat and Mass Transfer*, 51 (2008) 2267-2281.
- [30] A. Kosar, C. Kuo, Y. Peles, Suppression of Boiling Flow Oscillations in Parallel Microchannels by Inlet Restrictors, *Journal of Heat Transfer-transactions of The Asme*, 128 (2006) 251-260.
- [31] A. Mukherjee, S.G. Kandlikar, The effect of inlet constriction on bubble growth during flow boiling in microchannels, *International Journal of Heat and Mass Transfer*, 52 (2009) 5204-5212.
- [32] S. Kakac, B. Bon, A Review of two-phase flow dynamic instabilities in tube boiling systems, *International Journal of Heat & Mass Transfer*, 51 (2008) 399-433.
- [33] Y. Lv, G. Xia, L. Cheng, D. Ma, Experimental study on the pressure drop oscillation characteristics of the flow boiling instability with FC-72 in parallel rectangle microchannels, *International Communications in Heat and Mass Transfer*, 108 (2019) 104289.
- [34] G. Xia, Y. Cheng, L. Cheng, Y. Li, Heat transfer characteristics and flow visualization during flow boiling of acetone in semi-open multi-microchannels, *Heat Transfer Engineering*, (2018) 1-14.
- [35] H.-L. Wang, H.-C. Wu, S. Kong Wang, T.-C. Hung, R.-J. Yang, A study of mini-channel thermal module design for achieving high stability and high capability in electronic cooling, *Applied Thermal Engineering*, 51 (2013) 1144-1153.
- [36] Y. Jia, G. Xia, Y. Li, D. Ma, B. Cai, Heat transfer and fluid flow characteristics of combined microchannel with cone-shaped micro pin fins, *International Communications in Heat and Mass Transfer*, 92 (2018) 78-89.
- [37] C.T. Lu, C. Pan, Convective boiling in a parallel microchannel heat sink with a diverging cross section and artificial nucleation sites, *Experimental Thermal and Fluid Science*, 35 (2011) 810-815.

- [38] G. Xia, L. Chai, H. Wang, M. Zhou, Z. Cui, Optimum thermal design of microchannel heat sink with triangular reentrant cavities, *Applied Thermal Engineering*, 31 (2011) 1208-1219.
- [39] C. Dang, L. Jia, Q. Peng, L. Yin, Z. Qi, Comparative study of flow boiling heat transfer and pressure drop of HFE-7000 in continuous and segmented microchannels, *International Journal of Heat and Mass Transfer*, 148 (2020) 119038.
- [40] E.W. Lemmon , M.L. Huber, M.O. McLinden, NIST Reference Fluid Thermodynamic and Transport Properties – REFPROP, NIST Standard Reference Database 23 – Version 8.0, (2007).
- [41] G. Maranzana, I. Perry, D. Maillet, Mini- and micro-channels: influence of axial conduction in the walls, *International Journal of Heat and Mass Transfer*, 47 (2004) 3993-4004.
- [42] Y.T. Jia, G.D. Xia, L.X. Zong, D.D. Ma, Y.X. Tang, A comparative study of experimental flow boiling heat transfer and pressure drop characteristics in porous-wall microchannel heat sink, *International Journal of Heat and Mass Transfer*, 127 (2018) 818-833.
- [43] S.M. Zivi, Estimation of Steady-State Steam Void-Fraction by Means of the Principle of Minimum Entropy Production, *Trans.asme Ser.c*, 86 (1964) 247.
- [44] J.P. Holman, W.J. Gajda, *Experimental methods for engineers*, New York: McGraw-Hill, (1994).
- [45] T. Zhang, Y. Peles, J.T. Wen, T. Tong, J.-Y. Chang, R. Prasher, M.K. Jensen, Analysis and active control of pressure-drop flow instabilities in boiling microchannel systems, *International Journal of Heat and Mass Transfer*, 53 (2010) 2347-2360.
- [46] H.J. Lee, D.Y. Liu, S-C Yao, Flow instability of evaporative micro-channels, *International Journal of Heat and Mass Transfer* 53 (2010) 1740–1749

List of Table Captions

Table 1. Comparisons of structural parameters between MC 1 and MC 2.

Table 2. The thermophysical and transport properties of HFE-7100 at 101.3 kPa [39].

Table 3. The uncertainties of the measured and the derived parameters.

List of Figure Captions

Fig. 1 Schematic diagram of the flow boiling experimental system.

Fig. 2. Schematic diagram of assembled test section. (a) The structural parameters of microchannel substrate. (b) The assembly process of test section.

Fig. 3. Comparison of boiling curves and flow resistance characteristics in MC 1 and MC 2. (a) Boiling curves of HFE-7100 at the condition: $T_{in} = 25^{\circ}\text{C}$, $q_{eff} = 0 - 1080 \text{ kW/m}^2$ and $G = 608.8 - 1561.2 \text{ kg/m}^2\text{s}$.(b) Measured frictional pressure drops between the inlet and the outlet at the conditions of $T_{in} = 25^{\circ}\text{C}$, $q_{eff} = 0 - 1080 \text{ kW/m}^2$ and $G = 608.8 - 1561.2 \text{ kg/m}^2\text{s}$.

Fig. 4. Comparison of flow patterns in MC 1 and MC 2 at the condition: $G = 608.8 \text{ kg/m}^2\text{s}$ and $q_{eff} = 240.5 \text{ kW/m}^2$, and $T_{in} = 25^{\circ}\text{C}$. (a) The two-phase distribution in MC 1 between 2 to 4 mm and 6 to 8 mm.(b) The two-phase distribution in MC 2 between 2 to 4 mm and 6 to 8 mm.

Fig. 5. Comparison of heat transfer coefficients at outlet of MC 1 and MC 2 at the conditions of $T_{in} = 25^{\circ}\text{C}$, $q_{eff} = 0 - 1080 \text{ kW/m}^2$ and $G = 608.8 - 1561.2 \text{ kg/m}^2\text{s}$.

Fig. 6 Comparison of hydrodynamic characteristic curves and average negative slopes of HFE-7100 in MC 1 and MC 2. (a) Comparison of pressure drop characteristic curves of HFE-7100 in MC 1 and MC 2 at the condition: $T_{in} = 25^{\circ}\text{C}$, $q_{eff} = 426.1 - 672.8 \text{ kW/m}^2$ and $G_1 = 380 - 2500 \text{ kg/m}^2\text{s}$ and $G_2 = 710 - 3300 \text{ kg/m}^2\text{s}$.(b) Variation of absolute value of s_a in MC 1 and MC 2 at $q_{eff} = 200 - 800 \text{ kW/m}^2$.

Fig. 7 Oscillations of the main parameters in the unstable boiling at the conditions: $G = 1564.5 \text{ kg/m}^2\text{s}$, $q_{eff} = 672.8 \text{ kW/m}^2$, $V_{N2} = 5 \text{ ml}$ and $T_{in} = 25^{\circ}\text{C}$. (a) Variations of mass fluxes with time of HFE-7100 in MC 1 and MC 2. (b) Variations of pressure drops with time of HFE-7100 in MC 1 and MC 2. (c) Variations of the average wall temperatures and the fluid inlet and outlet temperatures of HFE-7100 in MC 1 and MC 2.

Fig. 8 Main parameters in the stable boiling at the condition: $G = 1564.5 \text{ kg/m}^2\text{s}$, $q_{eff} = 672.8 \text{ kW/m}^2$, $V_{N2} = 0 \text{ ml}$ and $T_{in} = 25^{\circ}\text{C}$. (a) Variations of mass fluxes with time of HFE-7100 in MC 1 and MC 2. (b) Variations of pressure drops with time of HFE-7100 in MC 1 and MC 2. (c) Variations of the average wall temperatures and the fluid inlet and outlet temperatures of HFE-7100 in MC 1 and MC 2.

Fig. 9 Comparisons of unstable flow boiling maps in MC 1 and MC 2. (a) The unstable flow boiling map in MC 1 at the conditions: $V_{N2} = 5 - 10 \text{ ml}$, $T_{in} = 25^{\circ}\text{C}$, $q_{eff} = 0 - 1200 \text{ kW/m}^2$ and $G = 211 - 2100 \text{ kg/m}^2\text{s}$.(b) The unstable flow boiling map in MC 2 at the conditions: $V_{N2} = 5 - 10 \text{ ml}$, $T_{in} = 25^{\circ}\text{C}$, $q_{eff} = 0 - 1200 \text{ kW/m}^2$ and $G = 211 - 2100 \text{ kg/m}^2\text{s}$.

Fig. 10 The simplified model of the flow boiling system with a compressive volume.

Fig. 11 Comparison of experimental and simulated results in MC 1 at the conditions: $V_{N2} = 5$ ml, $T_{in} = 25^\circ\text{C}$, $q_{eff} = 514.1$ kW/m² and $G = 1344.1$ kg/m²s. (a). The variations of measured mass flux in MC 1 at $t = 0 - 300$ s and $t = 900 - 1200$ s. (b). The variation of simulated mass flux in MC 1.

Fig. 12 The variation of R-squared with the negative slope in MC 1 and MC 2.

Table 1. Comparisons of structural parameters between MC 1 and MC 2.

Parameter	MC 1	MC 2
Number of channels, N	8	8
Width of channel, W_{mc} (μm)	220	220
Length of channel, L_{mc} (mm)	10	10
Depth of channel, D_{mc} (μm)	52	70
Hydraulic diameter, D_h (μm)	106	84.1
Cross-sectional area, A_{mc} (m^2)	1.54×10^{-8}	1.14×10^{-8}
Width of rib, W_{rib} (μm)	150	150
Aspect ratio	0.2364	0.3182

Table 2. The thermophysical and transport properties of HFE-7100 at 101.3 kPa [39].

Parameters	Value
T_{sat}	61 °C
ρ	1520 kg/m ³
c_p	1172 J/(kg·K)
h_{lg}	126 kJ/kg
λ	0.069 W/(m·K)

Table 3. The uncertainties of the measured and the derived parameters.

Measurement	Maximum relative uncertainty
T_w	0.1 K
T_{in}, T_{out}	0.05 K
p	5.22%
Δp	5.89%
G	4.85%
q_{eff}	4.95%
h	8.54%
x_{out}	4.22%

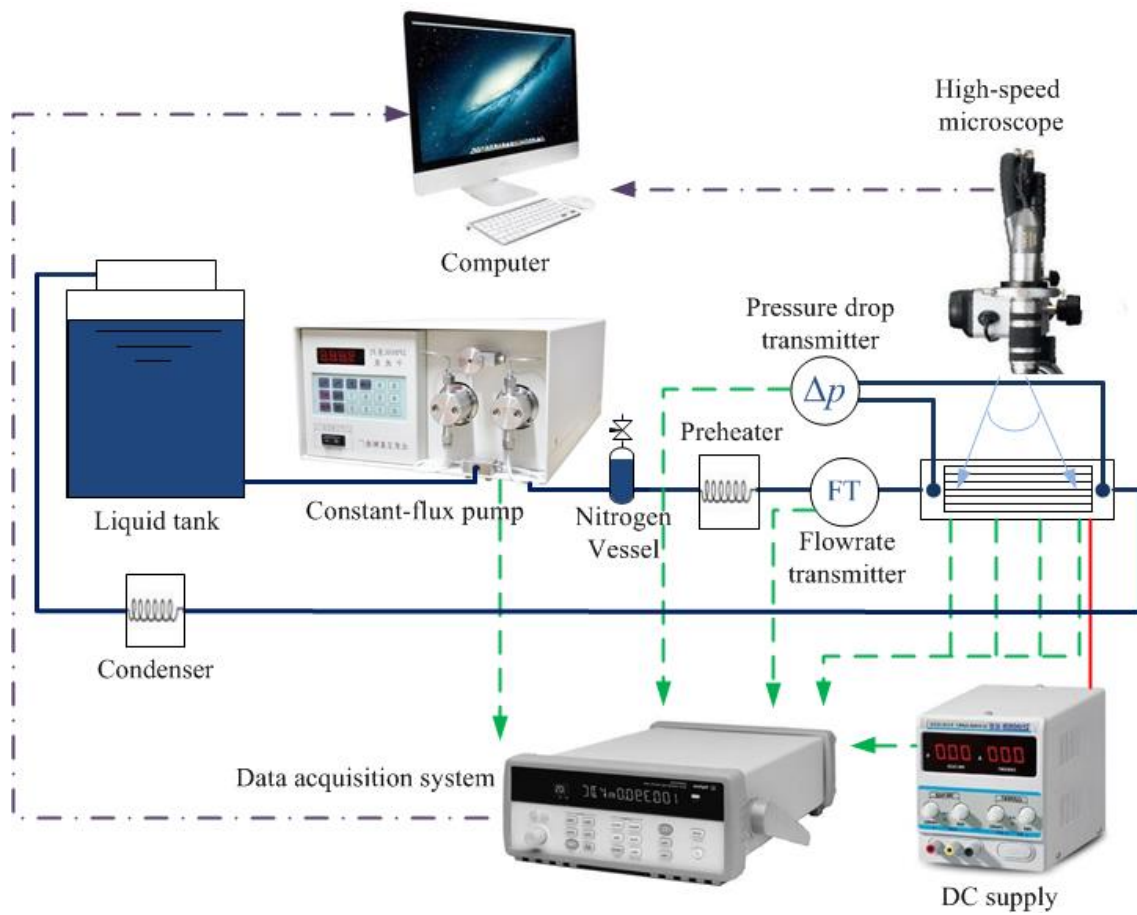
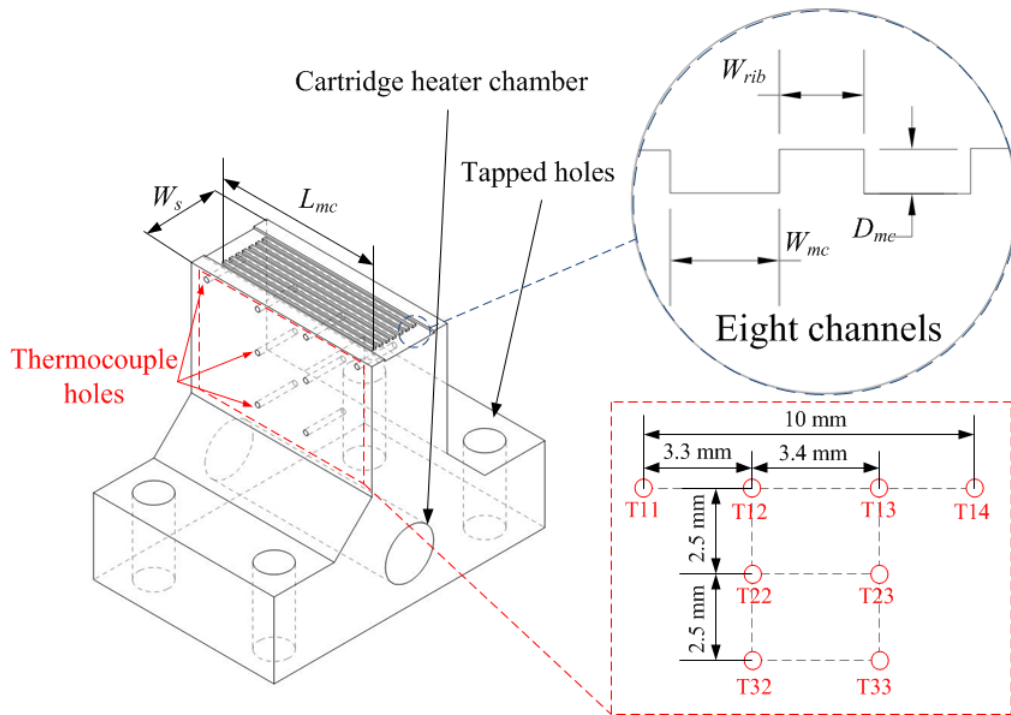
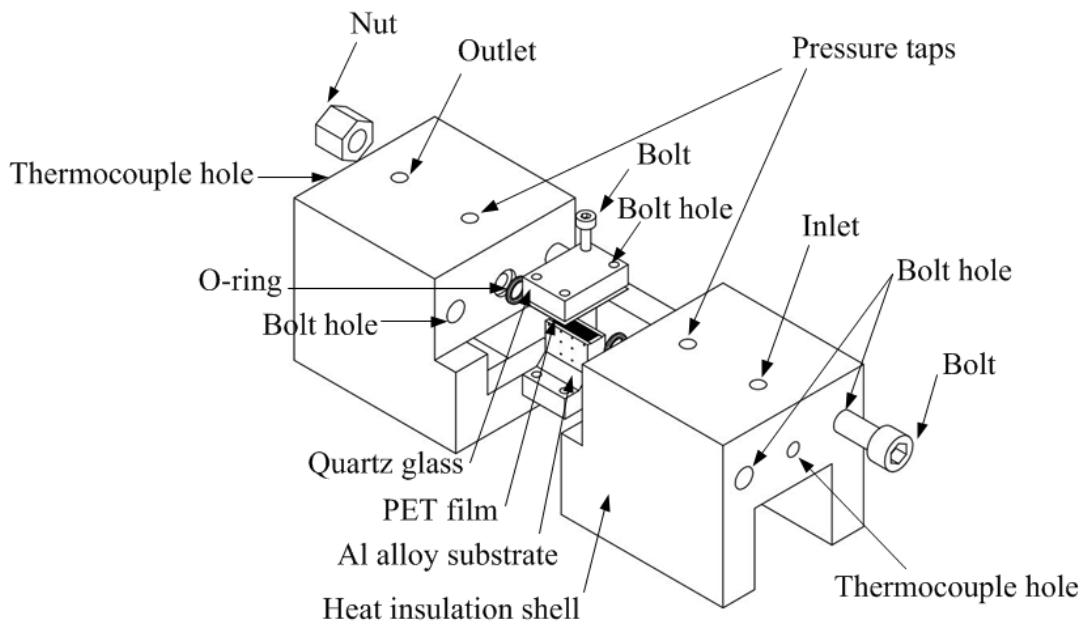


Fig. 1 Schematic diagram of the flow boiling experimental system.

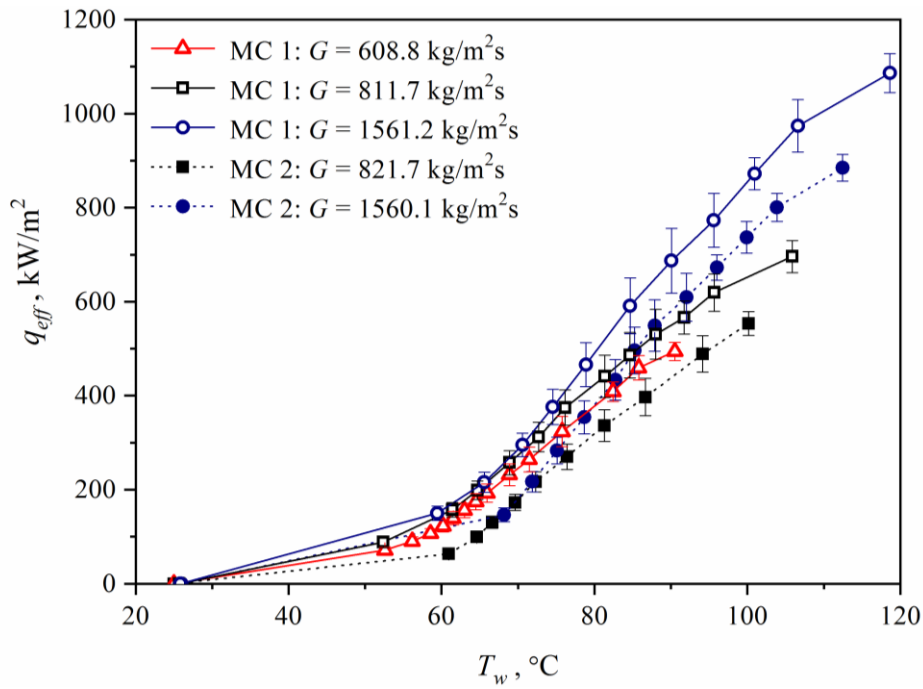


(a) The structural parameters of microchannel substrate

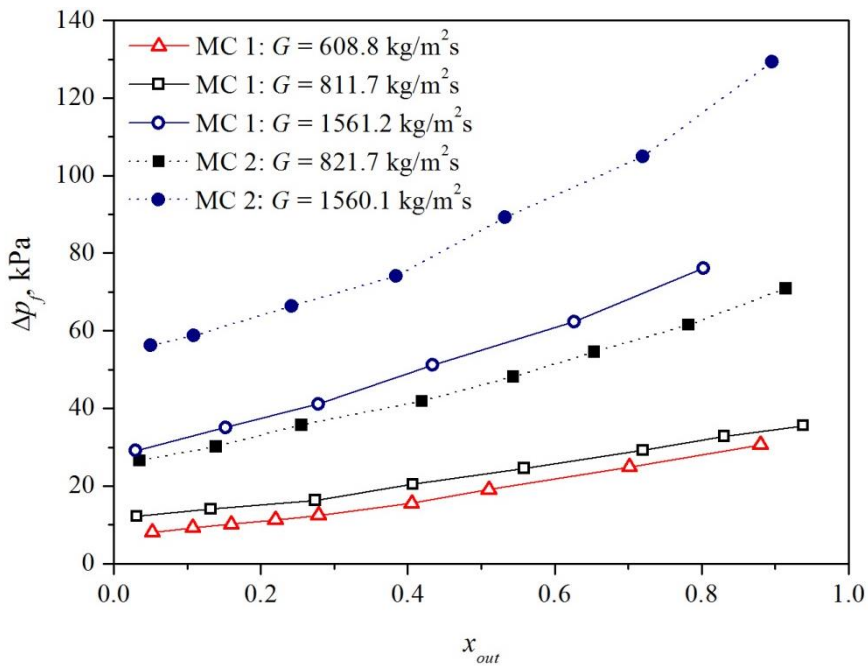


(b) The assembly process of test section

Fig. 2. Schematic diagram of assembled test section.

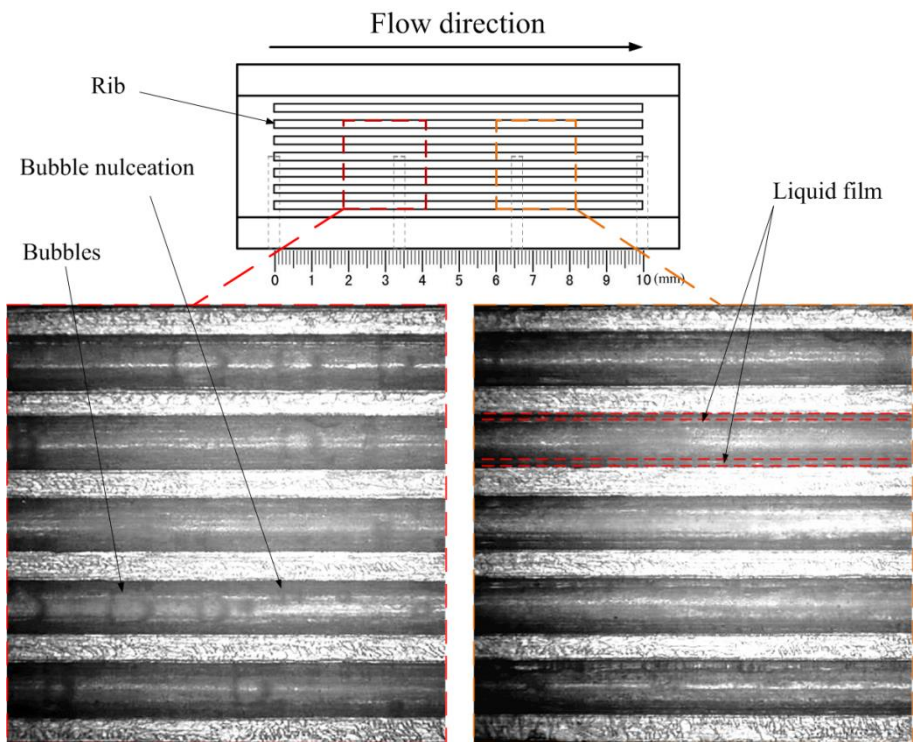


(a) Boiling curves of HFE-7100 at the condition: $T_{in} = 25^\circ\text{C}$, $q_{eff} = 0 - 1080$ kW/m² and $G = 608.8 - 1561.2$ kg/m²s.

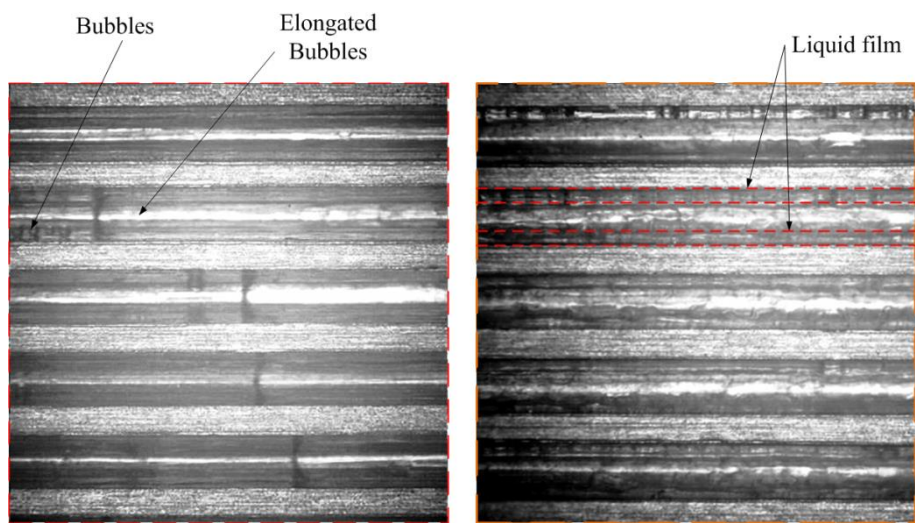


(b) Measured frictional pressure drops between the inlet and the outlet at the condition: $T_{in} = 25^\circ\text{C}$, $q_{eff} = 0 - 1080$ kW/m² and $G = 608.8 - 1561.2$ kg/m²s.

Fig. 3. Comparisons of boiling curves and flow resistance characteristics in MC 1 and MC 2.



(a) The two-phase distribution in MC 1 between 2 to 4 mm and 6 to 8 mm.



(b) The two-phase distribution in MC 2 between 2 to 4 mm and 6 to 8 mm.

Fig. 4. Comparison of flow patterns in MC 1 and MC 2 at the condition: $G = 608.8 \text{ kg/m}^2\text{s}$ and $q_{eff} = 240.5 \text{ kW/m}^2$, and $T_{in} = 25^\circ\text{C}$.

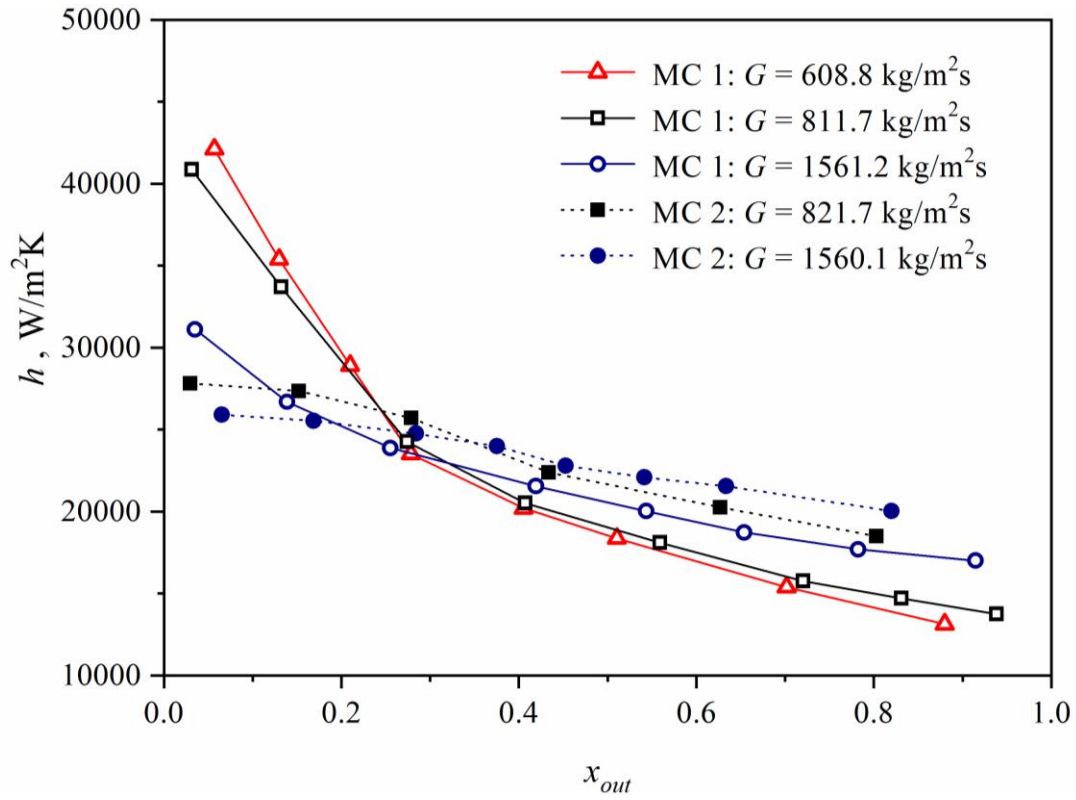
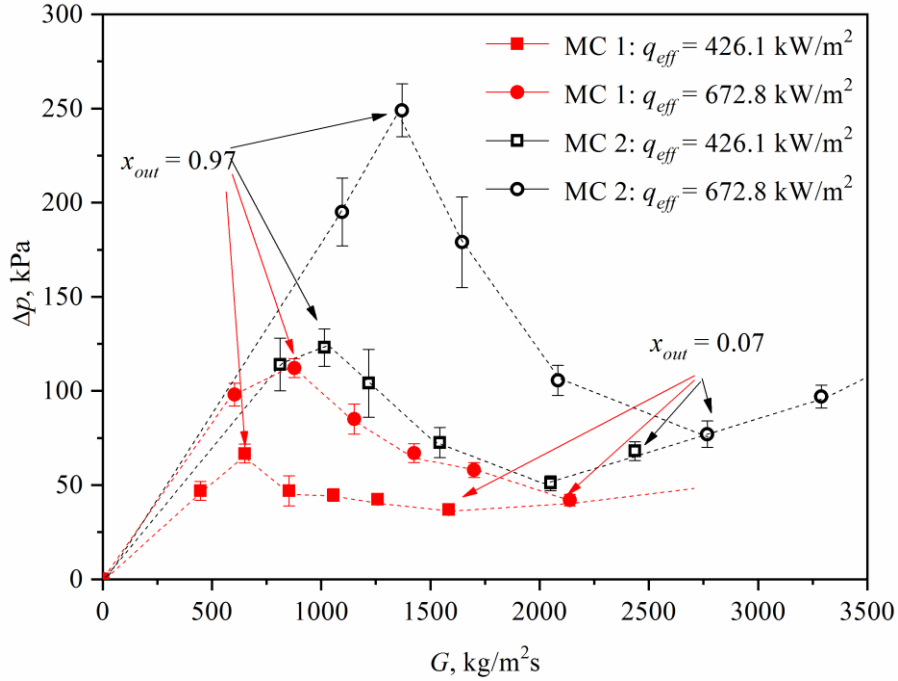
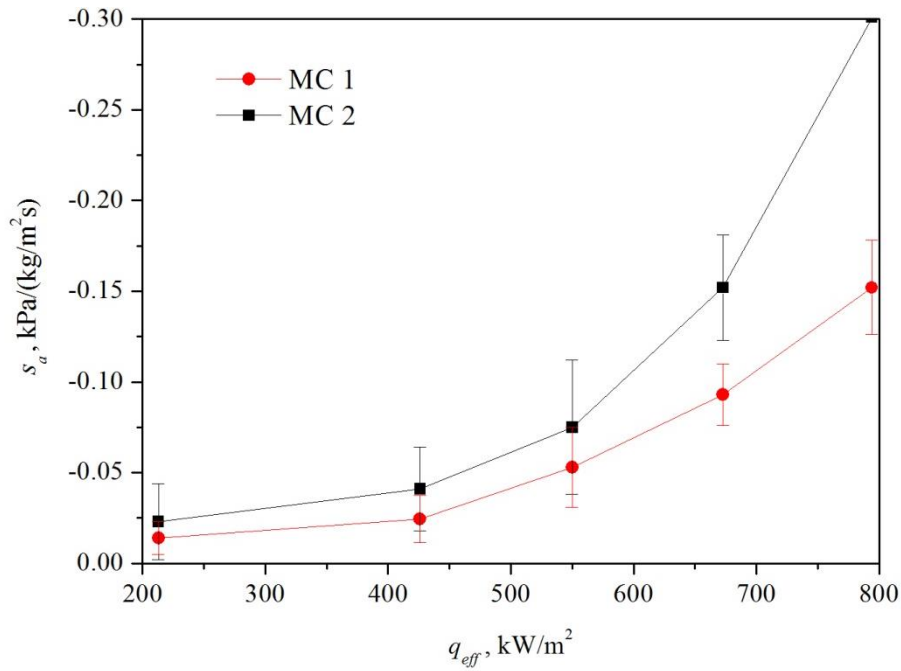


Fig. 5. Comparison of heat transfer coefficients at outlet of MC 1 and MC 2 at the condition: $T_{in} = 25^\circ\text{C}$, $q_{eff} = 0 - 1080 \text{ kW/m}^2$ and $G = 608.8 - 1561.2 \text{ kg/m}^2\text{s}$.

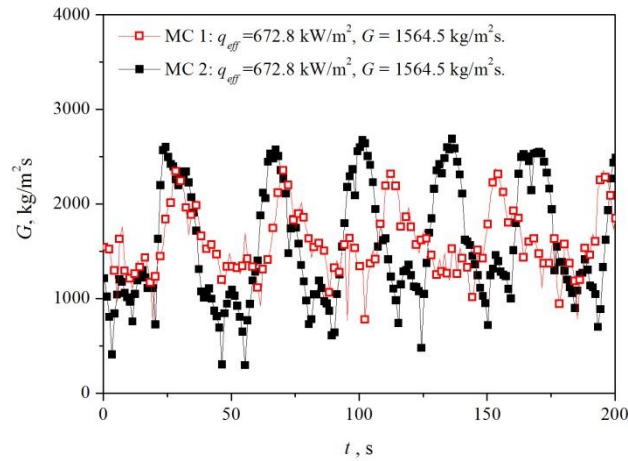


(a) Comparison of pressure drop characteristic curves of HFE-7100 in MC 1 and MC 2 at the condition: $T_{in} = 25^{\circ}\text{C}$, $q_{eff} = 426.1 - 672.8 \text{ kW/m}^2$ and $G_1 = 380 - 2500 \text{ kg/m}^2\text{s}$ and $G_2 = 710 - 3300 \text{ kg/m}^2\text{s}$.

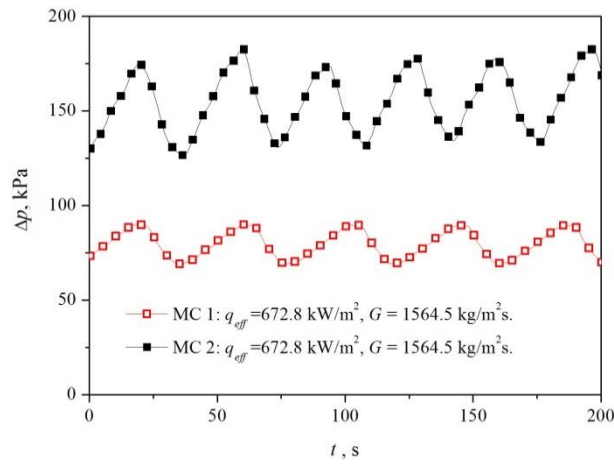


(b) Variation of absolute value of s_a in MC 1 and MC 2 at $q_{eff} = 200 - 800 \text{ kW/m}^2$.

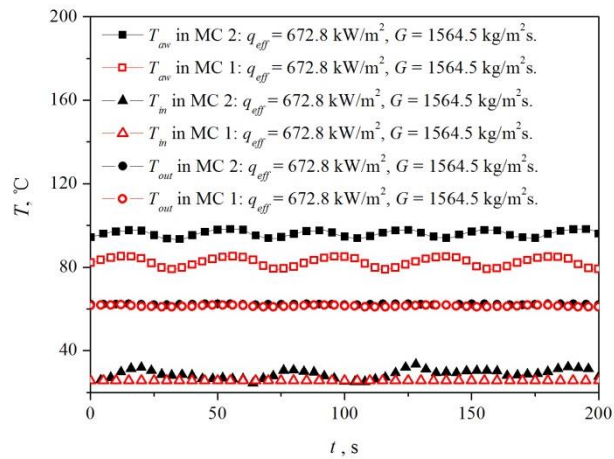
Fig. 6 Comparisons of hydrodynamic characteristic curves and average negative slopes of HFE-7100 in MC 1 and MC 2.



(a) Variations of mass fluxes with time of HFE-7100 in MC 1 and MC 2.

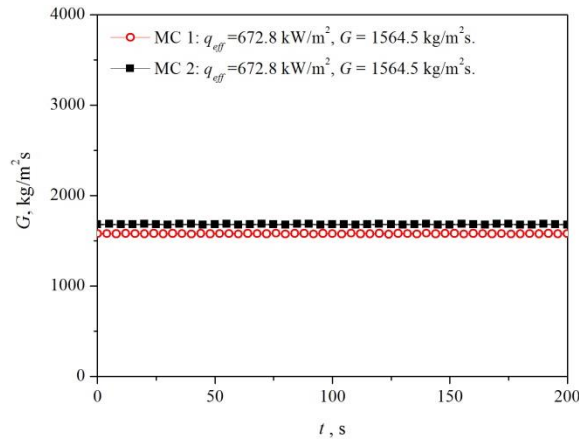


(b) Variations of pressure drops with time of HFE-7100 in MC 1 and MC 2.

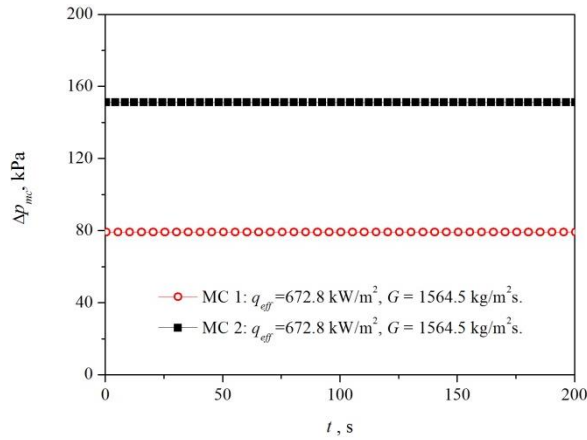


(c) Variations of the average wall temperatures and the fluid inlet and outlet temperatures of HFE-7100 in MC 1 and MC 2.

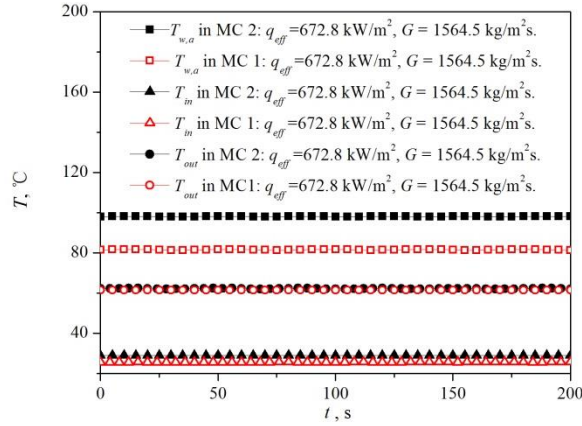
Fig. 7 Oscillations of the main parameters in the unstable boiling at the condition: $G = 1564.5 \text{ kg/m}^2\text{s}$, $q_{eff} = 672.8 \text{ kW/m}^2$, $V_{N_2} = 5 \text{ ml}$ and $T_{in} = 25^\circ\text{C}$.



(a) Variations of mass fluxes with time of HFE-7100 in MC 1 and MC 2.

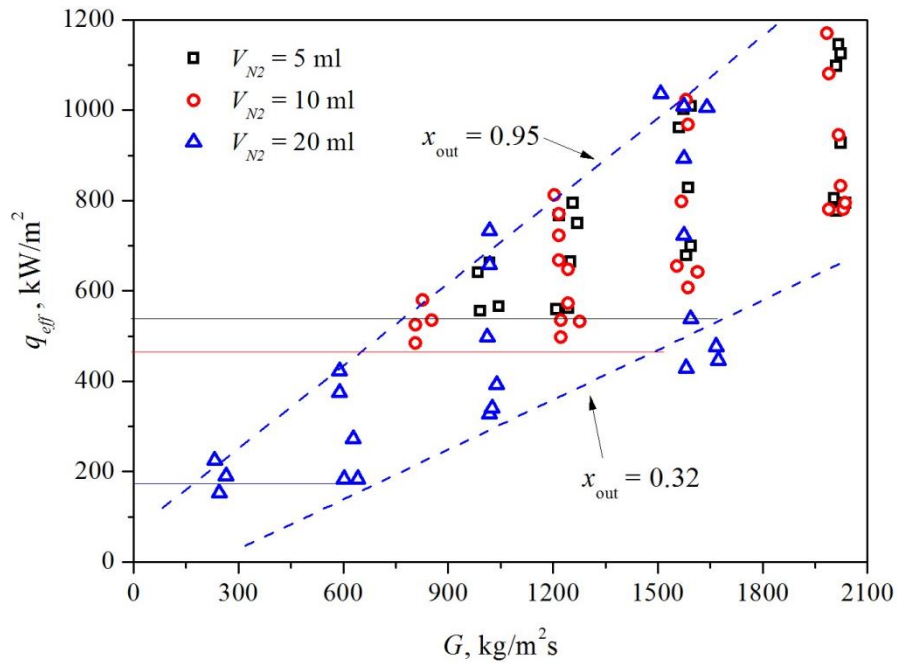


(b) Variations of pressure drops with time of HFE-7100 in MC 1 and MC 2.

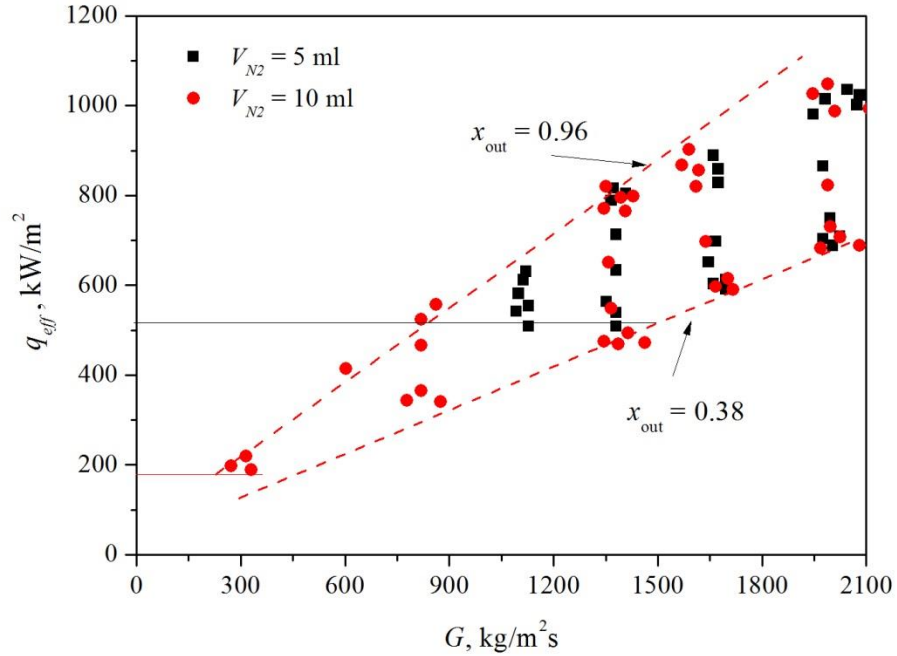


(c) Variations of the average wall temperatures and the fluid inlet and outlet temperatures of HFE-7100 in MC 1 and MC 2.

Fig. 8 Main parameters in the stable boiling at the condition: $G = 1564.5$ kg/m²s, $q_{eff} = 672.8$ kW/m², $V_{N2} = 0$ ml and $T_{in} = 25$ °C.



(a) The unstable flow boiling map in MC 1 at the condition: $V_{N_2} = 5 - 10$ ml, $T_{in} = 25^\circ\text{C}$, $q_{eff} = 0 - 1200$ kW/m² and $G = 211 - 2100$ kg/m²s.



(b) The unstable flow boiling map in MC 2 at the condition: $V_{N_2} = 5 - 10$ ml, $T_{in} = 25^\circ\text{C}$, $q_{eff} = 0 - 1200$ kW/m² and $G = 211 - 2100$ kg/m²s.

Fig. 9 Comparison of unstable flow boiling maps in MC 1 and MC 2.

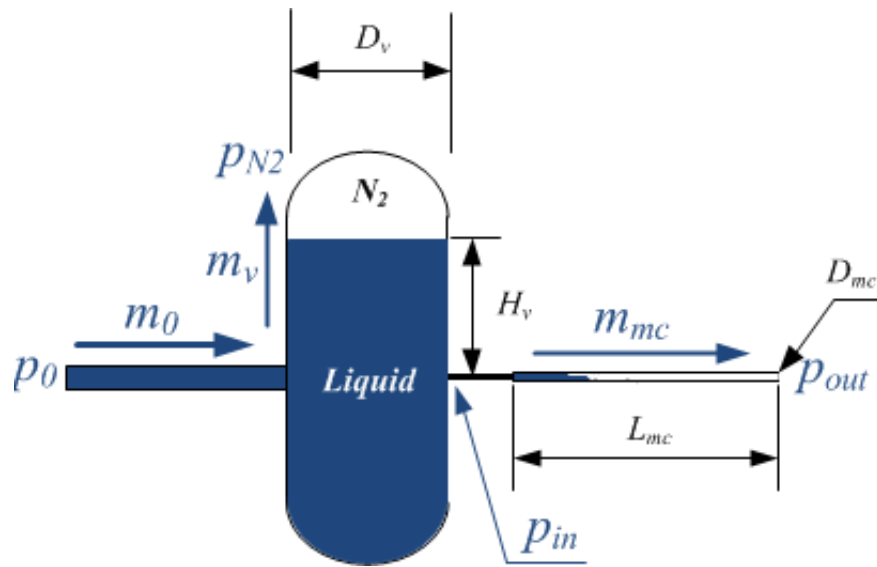
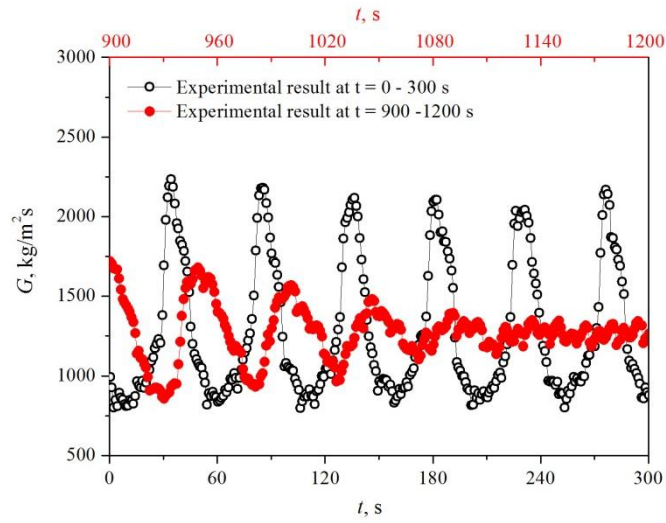
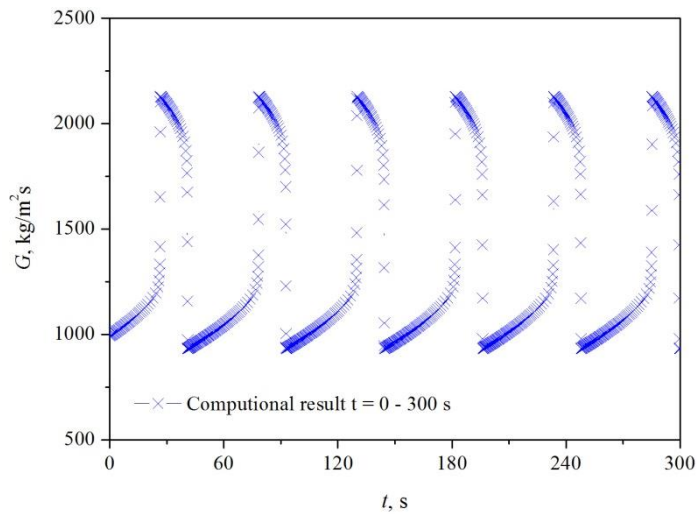


Fig. 10 The simplified model of the flow boiling system with a compressive volume.



(a) The variations of measured mass flux in MC 1 at $t = 0 - 300$ s and $t = 900 - 1200$ s.



(b) The variation of simulated mass flux in MC 1.

Fig. 11. Comparison of experimental and simulated results in MC 1 at the condition: $V_{N_2} = 5$ ml, $T_{in} = 25^\circ\text{C}$, $q_{eff} = 514.1$ kW/m² and $G = 1344.1$ kg/m²s.

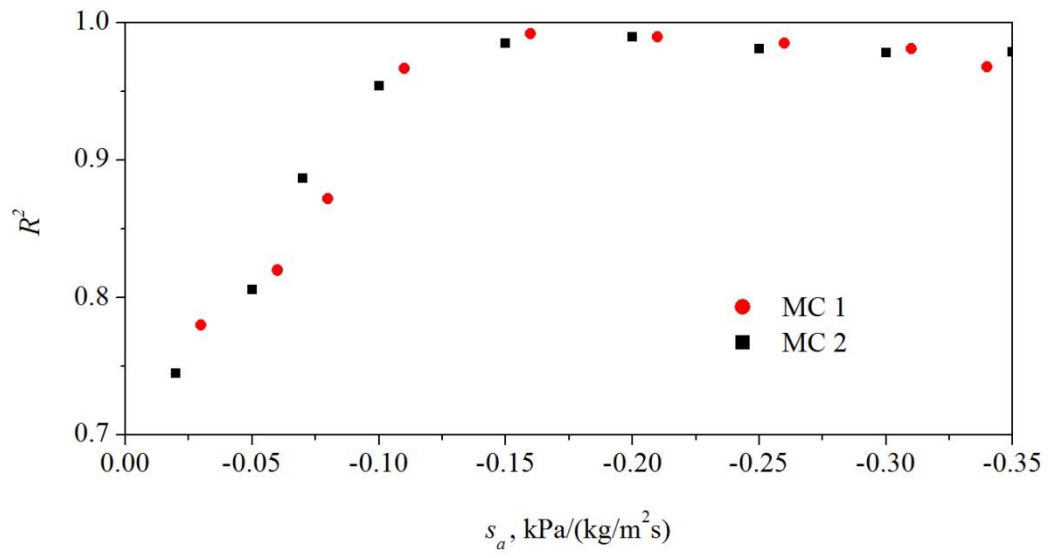


Fig. 12. The variation of R-squared with the negative slope in MC 1 and MC 2.